Available online at www.eccomasproceedia.org
Eccomas Proceedia COMPDYN (2023) 3404-3414

ECCOMAS
Proceedia

COMPDYN 2023
9th ECCOMAS Thematic Conference on
Computational Methods in Structural Dynamics and Earthquake Engineering
M. Papadrakakis, M. Fragiadakis (eds.)
Athens, Greece, 12-14 June 2023

STRUCTURAL DEFORMATION RECONSTRUCTION USING THE HYBRID SHELL-BEAM INVERSE FINITE ELEMENT METHOD: EXPERIMENTAL APPLICATION ON A THIN-WALLED STIFFENED PANEL

Marco Esposito[1], Rinto Roy[2], Marco Gherlone[1] and Cecilia Surace[2]

[1]Department of Mechanical and Aerospace Engineering, Politecnico di Torino
Corso Duca degli Abruzzi, 24, Torino, Italy
e-mail: {marco.esposito, marco.gherlone}@polito.it

[2] Department of Structural, Geotechnical and Building Engineering, Politecnico di Torino
Corso Duca degli Abruzzi, 24, Torino, Italy
e-mail: {rinto.roy, cecilia.surace}@polito.it

Abstract. *The continuous developments in the field of Structural Health Monitoring (SHM) and the simultaneous push toward the realization of the digital twin paradigm has generated a strong request for the on-line monitoring of structural responses that are usually difficult to measure through direct sensing. Among these responses, the displacements, and the stresses that can be derived from them, play a crucial role. The indirect computation of the displacement field from easily measurable surface strains, known as shape sensing, has inspired the definition of an inverse formulation of the Finite Element Method, the iFEM. As for the standard FEM, this approach is based on the discretization of the structural domain with finite elements. Therefore, 2D inverse shell elements and 1D inverse beam elements have been separately proposed and tested for the shape sensing of plate and beam-like structures, respectively. However, especially in aerospace applications, thin-walled stiffened panels are often adopted. These structures can be discretized using hybrid shell-beam models. In this work, the iFEM hybrid shell-beam formulation is applied for the first time to the experimental shape sensing of an aluminum stiffened panel instrumented with strain sensing optic fibres. The displacements' reconstruction is compared to the one obtained with a high-fidelity shell-only inverse model of the same structure. The comparison shows that the hybrid iFEM is capable of the same level of accuracy of the shell-only one, using a more computationally efficient model with less degrees of freedoms. These results prove that the proposed hybrid formulation is a valuable displacements' monitoring tool for applications where computational efficiency is paramount and the level of detail achieved by low-fidelity hybrid models is sufficient, as it occurs in aeroelastic models.*

Keywords: Inverse Methods, Shape Sensing, iFEM, Beam-Shell Models, Stiffened Panel, Experimental validation.

ISSN:2623-3347
Peer-review under responsibility of the organizing committee of COMPDYN 2023.
doi: 10.7712/120123.10648.20653

1 INTRODUCTION

Structural Health Monitoring (SHM) is rapidly imposing itself as a crucial tool for the future of structural design in every technological area where damages and failures can occur. Within the SHM framework, different tools and technologies have been developed, depending on the specific characteristics of the structure that they are designed to monitor. In particular, several techniques for the monitoring of the displacements during the service life of a structure are rapidly developing [1]. The reconstruction of the displacement field from discrete strain sensors is defined as shape sensing. The shape sensing methods represent an important tool to improve the efficiency of the structural maintenance operations [2] and can also be implemented for damage detection activities[3, 4]. Among the existing approaches, the inverse Finite Element Method (iFEM) has emerged has one of the most accurate and efficient [5].

The iFEM is based on an inverse formulation of the Finite Element Method that allows, from a sparse set of strain measures, to compute the displacement field that induced those strains [6]. As for the standard FEM, it is based on the discretization of the structural domain with finite elements. Therefore, several inverse finite elements have been developed, with characteristics that adapt to different structural components. One-dimensional inverse elements for the analysis of beam structures have been developed in [7], whereas two-dimensional elements for the analysis of thin plates have been introduced in [8].

Several applications of the iFEM have involved the separate use of either 1D or 2D models for the displacement reconstruction of beam-like or thin-walled structures. Beam inverse elements have been successfully used for the shape sensing of sub-sea [9] and buried [10] pipelines. In [11] an inverse 1D element based on the Timoshenko beam theory has been applied to the displacement reconstruction of an airfoil beam. On the other hand, 2D shell inverse elements have been successfully involved in the shape sensing of aerospace and marine structures. In [12] 2D quad inverse elements have been used to model and analyse an aeronautical stiffened panel. In [13] the iFEM has been applied on the displacement and stress monitoring of a a capsize bulk carrier, using inverse quad elements.

Although a consistent research effort has concerned the development of different formulations and applications of 2D and 1D inverse elements, the application of beam and shell elements within the same model has never been explored. In the case of thin-walled stiffened structures, the standard FE structural analysis often involves the use hybrid shell-beam models, where the shell elements are used to simulate the thin-walled part and the beam elements are associated to the stiffeners. In this work, for the first time, the same approach is adopted for the experimental shape sensing of an aluminium stiffened panel. In fact, the displacement reconstruction is performed by discretizing the panel with quadrilateral inverse elements and the stiffeners with beam inverse elements. The results obtained with the hybrid shell-beam model are compared with the one computed trough the use of a more detailed standard shell-only inverse model. The study proves that the hybrid model is able to reach the same accuracy of the detailed model with a less computationally demanding model and with a slightly reduced number strain sensors.

The paper is structured as follows. In Section 2, the hybrid iFEM formulation is briefly described. In Section 3 the experimental setup and the structure object of the analysis are presented. The inverse models and the strain sensors' configurations for the shape sensing are introduced in Section 4. The results of the experimental campaign are reported in Section 5. Finally, the concluding remarks and the recommendations for the future development of the hybrid models are included in Section 6.

2 Hybrid inverse shell-beam formulation

The inverse Finite Element Method is based on the discretization of the structural domain with finite elements. This discretization leads to the formulation of the displacement field in terms of the shape functions and of the nodal degrees of freedom.

Once the discretized displacement field is defined, the dicretized strain field can be easily obtained by deriving the shape functions, thus obtaining the expression of the strain field in terms of the nodal values of the nodal degrees of freedom:

$$\mathbf{e}(\mathbf{u}^e) = \mathbf{B}\mathbf{u}^e \tag{1}$$

where $\mathbf{B}^s$ is a matrix of shape function derivatives and $\mathbf{u}^e$ is the vector of nodal DOF of element e of the inverse model. $\mathbf{B}$, $\mathbf{u}_e$ and the strain components that define the vector $\mathbf{e}(\mathbf{u}^e)$ depend on the kind and formulation of the selected inverse element.

This analytical expression of the strain field can be compared with the one experimentally measured at discrete locations, in order to compute the nodal degrees of freedom value that best fit the measured strain field. The procedure is obtained by defining an error functional. For the beam element e, the error functional $\mathbf{\Phi}_b^e$ is defined as:

$$\Phi_b^e(\mathbf{u}_b^e) = \sum_{k=1}^{6} \lambda_k^b w_k^b \sum_{i=1}^{N} \frac{l_e}{N} \left[e_k(x_i) - (e_k^\varepsilon)_i\right]^2 \tag{2}$$

where $e_k(x_i)$ is the k-th analytical sectional strain computed at the section identified by the x_i axial coordinate, $(e_k^\varepsilon)_i$ is the k-th measured sectional strain coming from a sensor at the same axial location, N is the number of sections within the beam element where the strains are measured and l_e is the length of the beam element. The index k identifies the six sectional strains that define the strain field for a Timoshenko beam, namely: axial stretching ($k = 1$), bending curvatures ($k = 2, 3$), transverse shear ($k = 4, 5$) and torsional strain ($k = 6$). λ_k^b are coefficients that guarantee the dimensional consistency between the different sectional strains. w_k^b is a weight used to take into account for sparse strain sensors configurations. It is set to 1 if the corresponding sectional strain is measured or to a small vale (10^{-5}) if it is not. For the application concerning this work, only sensors that measure axial stretching and bending curvatures are considered. Therefore, for sensorized beam elements, the value of w_k^b for ($k = 4, 5, 6$) is set to 10^{-5} and for ($k = 1, 2, 3$) is set to 1. On the the other hand, for unsensorized elements all the weights are set to 10^{-5}. A more detailed description of the iFEM formulation for the beam elements can be found in [11].

Using the same approach, the error functional can also be defined for shell elements. In this case the functional $\mathbf{\Phi}_p^e$ is defined as:

$$\Phi_p^e(\mathbf{u}_p^e) = \sum_{k=1}^{8} \lambda_k^p w_k^p \iint_{A^e} [e_k(\mathbf{u}^e) - e_k^\varepsilon]^2 dxdy \tag{3}$$

where $e_k(\mathbf{u}^e)$ is the k-th analytical strain measure, e_k^ε is the k-th strain measure derived from sensors' measurements and A^e is the area of the shell element. In this case, the k index identifies the eight strain measures that define the strain field for a Mindlin plate, namely: the membrane strain ($k = 1, 2, 3$), the bending curvatures ($k = 4, 5, 6$) and the transverse shear strains ($k = 7, 8$) of the plate. In this case, the λ_k^p and w_k^p coefficient assume the same role as λ_k^b and w_k^b. Since the transverse shear strains are not measurable through strain sensors, the values of w_k^p

for ($k = 7, 8$) is always set to 10^{-5}. The detailed formulation of the inverse shell elements can be found in [14].

The minimization of the functional with respect to the nodal DOFs for each element generates a system of linear equations. In the case of a hybrid model, the simultaneous minimization of the error functional for the beam and shell elements needs to be performed:

$$\frac{\partial \Phi_b^e(\mathbf{u}_b^e)}{\partial \mathbf{u}_b^e} = \mathbf{k}_b^e \mathbf{u}_b^e - \mathbf{f}_b^e = 0 \tag{4}$$

$$\frac{\partial \Phi_p^e(\mathbf{u}_p^e)}{\partial \mathbf{u}_p^e} = \mathbf{k}_p^e \mathbf{u}_p^e - \mathbf{f}_p^e = 0 \tag{5}$$

The standard FE assembly procedure for all the N^e elements, taking into account for the necessary transformations from the local DOFs of the elements to the global ones, generates the global matrices:

$$\begin{aligned} Assembly(\mathbf{k}_b^e; \mathbf{k}_p^e)_{e=1:N^e} &\rightarrow \mathbf{K} \\ Assembly(\mathbf{f}_b^e; \mathbf{f}_p^e)_{e=1:N^e} &\rightarrow \mathbf{F} \end{aligned} \tag{6}$$

where $\mathbf{K}$ is a matrix depending on the shape functions and strain sensor locations, whereas $\mathbf{F}$ is a vector incorporating the measured strains. The matrix $\mathbf{K}$ is a well-conditioned square matrix that, upon enforcement of the displacement boundary conditions, can be inverted to compute the vector of the global DOFs, $\mathbf{U}$, that best fit in a least-square sense the measured strains:

$$\mathbf{U} = \mathbf{K}^{-1}\mathbf{F} \tag{7}$$

It is important to highlight that the iFEM is only based on the strain-displacement relationship and, therefore, does not require any knowledge of the material characteristics or the loading condition of the monitored structure.

3 Experimental setup

The test case for the experimental validation of the hybrid shell-beam inverse model is an aluminium stiffened panel. The panel is made of a Aluminium-Lithium alloy, whose mechanical characteristics are reported in Table 1. The geometry of the panel is presented in Fig. 1 and 2. It

	Al-Li alloy
$E\ [MPa]$	75,958
ν	0.3
$\rho\ [g/cm^3]$	2.78

Table 1: Mechanical properties of the Aluminium-Lithium alloy.

has three L-section stringers and it is 3.92 mm thick, except for four areas between the stringers where the thickness is reduced to 1.91 mm.

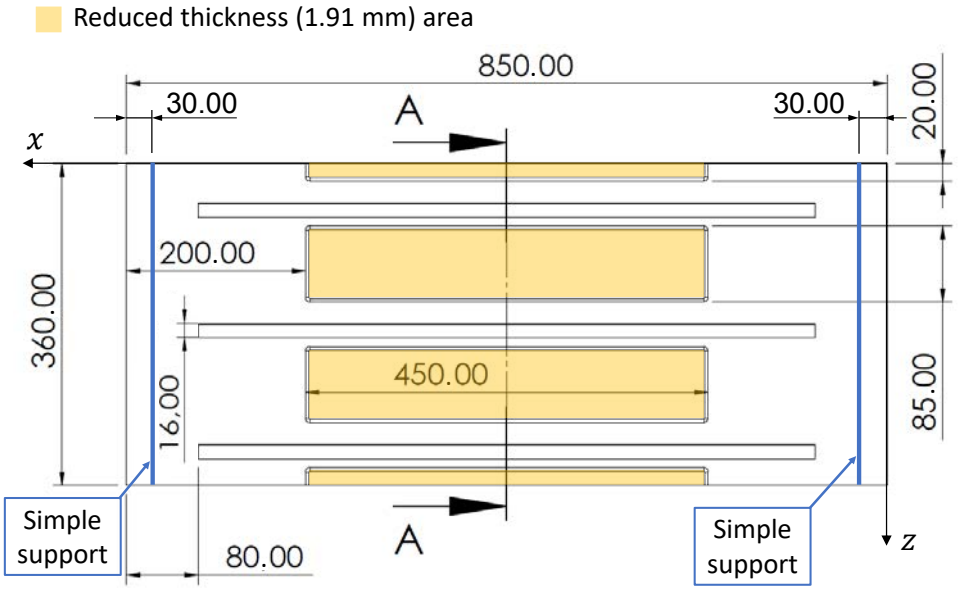

Figure 1: Geometry of the panel - Bottom view of the panel. All dimensions are expressed in mm.

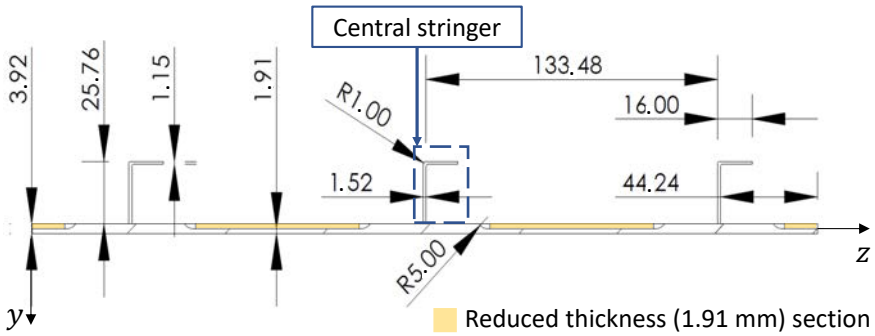

Figure 2: Section A - Section view of the panel. The section A is defined in Figure 1. All dimensions are expressed in mm.

The panel is tested in a simply supported condition. The simple support is obtained by placing the panel between two half-cylinder iron bars that constrain the transverse displacement but allow the rotations (Figure 3). The two supports are parallel to the shortest edges and located at a distance of 30 mm from them. The panel is loaded on the flat surface with a concentrated transverse force. The load is transmitted to the midpoint of the panel through an iron sphere that is pushed downwards by a iron bar installed on two threaded bars. By tightening two bolts on the threaded bars, the iron bar is pushed down and the load is transmitted to the panel by the sphere. The threaded bars are instrumented with two load cells in order to measure the applied load. The experimental setup is shown in Figure 4.

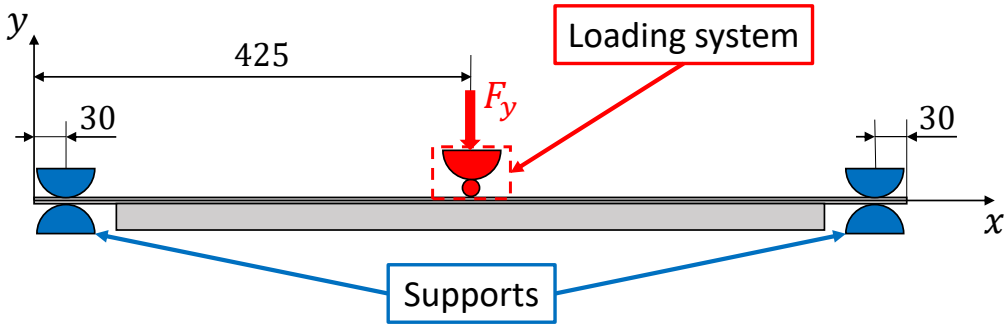

Figure 3: Loading system and boundary conditions. All dimensions are expressed in mm.

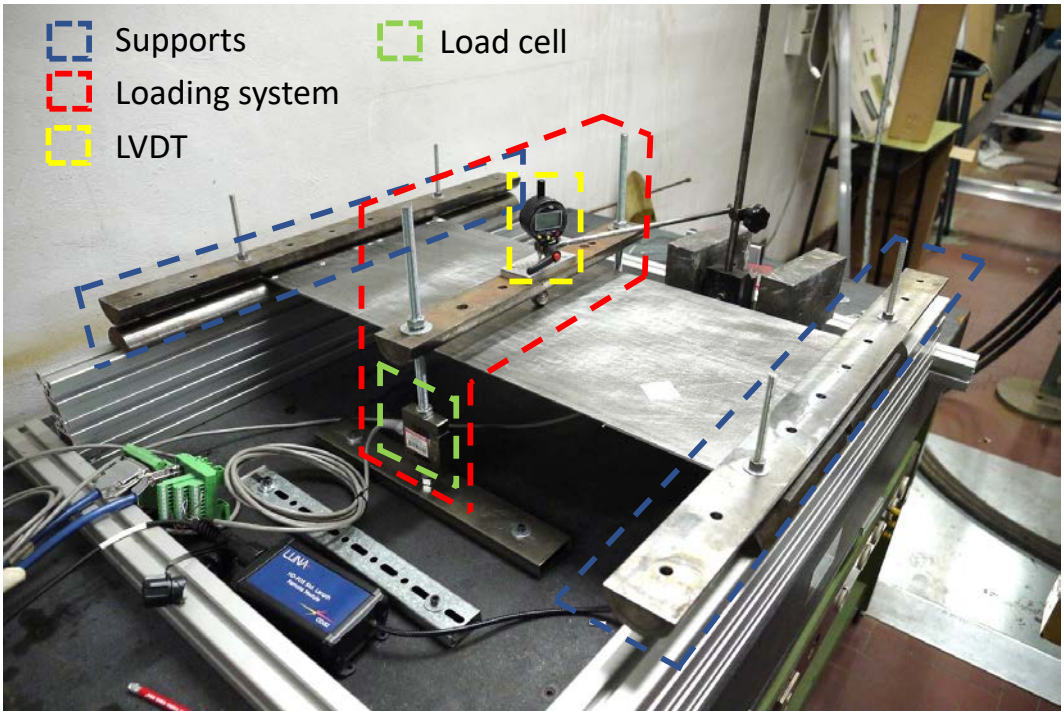

Figure 4: Experimental setup - The test is performed using four LVDTs. In the picture only one of the four LVDTs is shown. The detailed configuration of the LVDTs is presented in Fig. 7

4 Inverse models and strain sensors

Two inverse models of the structure have been realized. The first one is a standard shell-only model, made of 914 inverse quad elements and 978 nodes, accounting for a total of 5868 DOFs (Figure 5a). In this case, all the components of the panel are simulated using quad shell elements. This model is used as benchmark to evaluate the accuracy and the efficiency of the hybrid model. The focus of this work, the hybrid model, on the other hand, is constituted of 608 inverse quad elements to simulate the panel and of 102 inverse beam elements to model the three stiffeners (Figure 5b). The model has 663 nodes and 3978 DOFs. The reduced number of DOFs indicates that this model is less computationally demanding than the shell-only one.

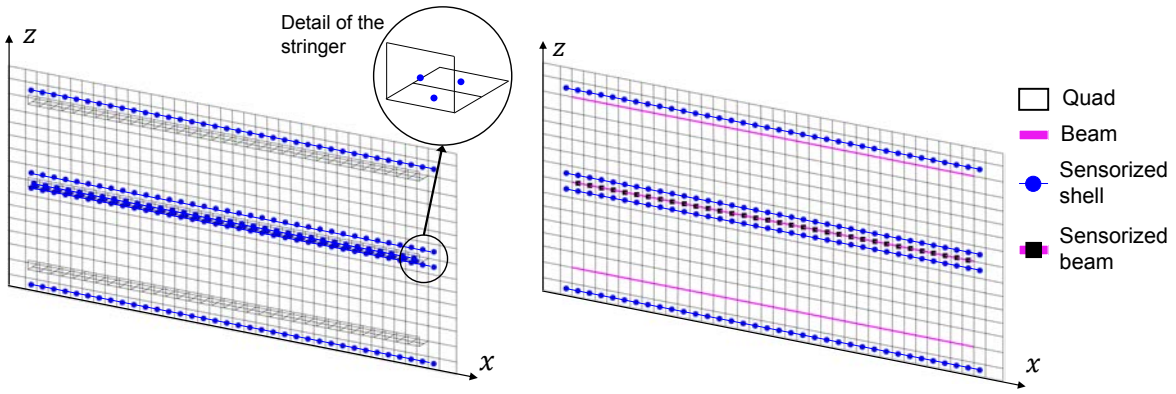

(a) Shell-only model (b) Hybrid model

Figure 5: Inverse models and strain sensors' configurations - The two inverse models are shown. The sensorized elements illustrated in the figures consider uni-axial strain sensors along the x direction.

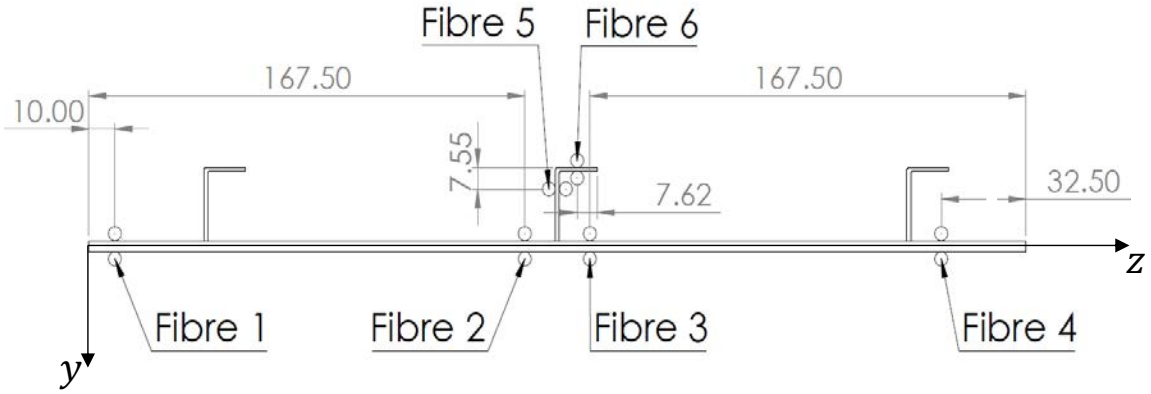

Figure 6: Distribution of the fibres on the panel. The fibres are numbered considering only one side of the back-to-back configuration. All dimensions are expressed in mm.

The strain sensors' configuration for the two models is illustrated in Figure 5. The configuration only considers mono-axial strain measurements in the direction of the longest edge of the panel. The configurations are experimentally obtained by instrumenting the panel with fibre optic strain sensors based on the Rayleigh scattering. These sensors allow the measurement of the strain along the fibre direction with an impressive density of a strain measurement every 1.3 mm. The strain sensors' configuration adopted for this test includes six sensing lines along the panel's length in a back-to-back configuration, i.e. every line on one side of the panel has a corresponding line on the other side as well. The six sensing lines of fibre are distributed on the panel as illustrated in Figure 6. The first four lines (Fibre 1-4), that are installed on the panel, are common to both the models' configurations. They guarantee, thanks to the sensors' density of the fibre, the sensing of the mono-axial strain in the x direction at the centroid of every sensorized shell element on both the bottom and top surface, as prescribed by the inverse

shell's formulation. For the shell-only model, Fibre 5 and 6, in the back-to back configuration, allow the sensorization of the shell elements simulating the central stringer, in the same way described for the panel. On the other hand, for the hybrid model, the sensorization of the beam elements, relative to the central stinger, only need three sensing lines, Fibre 5 in the back-to-back configuration, and Fibre 6, without the internal sensing line. In fact, the full sensorization of each beam element is obtained by measuring the three axial strains, coming from the fibres, at two sections($l_e/4$; $3l_e/4$) along the element's length (l_e).

To summarize, the hybrid model has less DOFs with respect to the shell-only one and, therefore, is less computationally demanding. Morover, because of the beam elements' formulation, to obtain a strain sensors' configuration that monitors the same components of the structure, slightly fewer sensors than the shell-only model are needed.

5 Experimental Results

The experimental test is performed by loading the structure with a concentrated load of 879 N. To assess the accuracy of the shape sensing for the two models, during the test, the transverse deflections of the panel in four points are experimentally measured with LVDTs. One LVDT is placed on the loading system and measures the maximum transverse deflection of the panel. The other three LVDTs are randomly distributed over the flat surface of the panel, as shown in Figure 7.

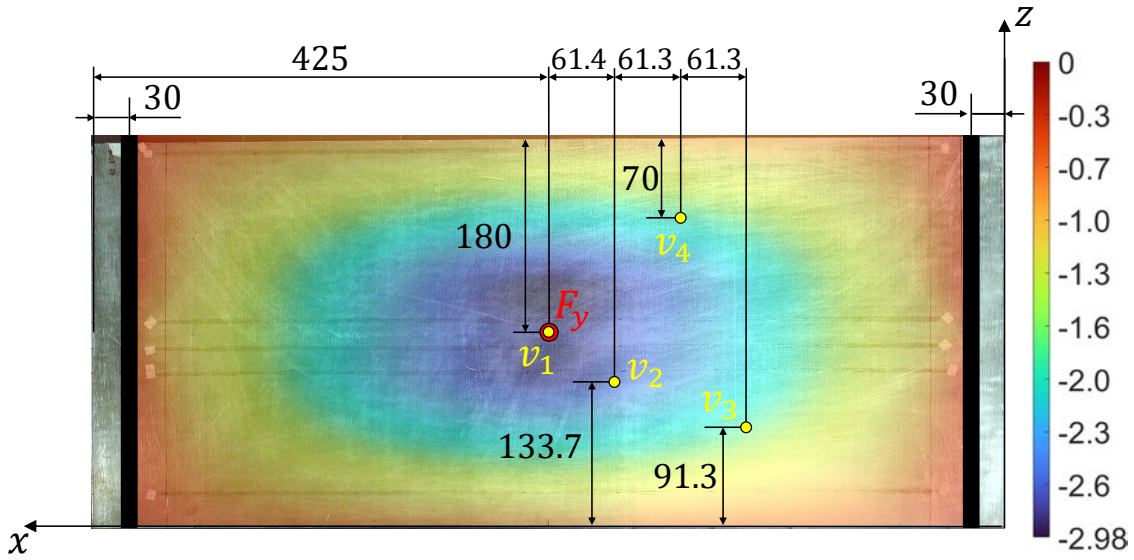

Figure 7: Results and LVDTs' configuration - The contour plot of the reconstructed transverse deflection with the hybrid model is shown on the panel. Moreover the location of the four LVDTs is presented. All dimensions are expressed in mm.

Once the test is performed, the data from the optic fibre are collected to perform the iFEM analysis with the two models. The reconstruction of the transverse deflection for the whole panel, using the hybrid model, is presented in Figure 7. More in details, the experimental values of the measured deflections and the reconstructed values for the two inverse models are reported in Table 2. In the table, the percentage errors and the mean absolute percentage errors are also reported. From the analysis of these values, it can be noted that the average accuracy

of the two model is strongly correlated. Both models show an extremely low value of the mean error, that is lower than 2%. Moreover, also the evaluation of the errors relative to the single displacements shows that the level of accuracy of the hybrid model is totally comparable with the one obtained by the shell-only model. In fact, although small differences exist for the single values, all the errors, for both the considered cases, are comprised between 0.6% and 2.0%.

	Experimental	Hybrid iFEM	Shell-only iFEM
$F_y\ [N]$	879		
$v_1\ [mm]$	3.030	2.983	2.988
$(\%Err_{v_1})$		(-1.5%)	(-1.4%)
$v_2\ [mm]$	2.698	2.715	2.661
$(\%Err_{v_2})$		(+0.6%)	(-1.4%)
$v_3\ [mm]$	1.670	1.652	1.636
$(\%Err_{v_3})$		(-1.1%)	(-2.0%)
$v_4\ [mm]$	1.691	1.657	1.660
$(\%Err_{v_4})$		(-2.0%)	(-1.8%)
$\mu(\lvert\%Err\rvert)$		1.3%	1.6%

Table 2: Shape sensing results - In parenthesis, the percentage errors with respect to the experimental values are reported. The errors are computed considering the absolute value of the displacements. Moreover the mean absolute value of the percentage error is reported ($\mu(\lvert\%Err\rvert)$).

6 Conclusions

In this work, an hybrid shell-beam iFEM model is experimentally tested on the shape sensing of an aluminium stiffened panel. The model is constituted of shell inverse quad elements for the modelization of the panel and of beam inverse elements for the simulation of the L-section stringers. The accuracy of the hybrid model is compared with the one obtained using a standard shell-only model, where also the stiffeners are modeled using inverse quad elements. The configuration of the strain sensors adopted to perform the shape sensing for the two models is equivalent in terms of sensorized components. In fact, four strain sensing lines are installed on the panel and the central stringer is instrumented with strain sensing optic fibres. However, because of the different modelization of the stringer, the sensorization of this component needs one less sensing line for the beam elements belonging to the hybrid model. Therefore, the hybrid model has a little advantage in terms of required sensors. Another advantage of the hybrid model is related to the computational efficiency. This model has a reduced number of nodes and, as a consequence a smaller amount of Degrees of Freedom to be computed.

The experimental campaign proves that the accuracy in the reconstruction of the displacements obtained by the hybrid model is comparable with the one achieved by the shell-only model. In fact, both the models show the same excellent level of the error in the reconstruction of the displacements, never exceeding the value of 2%. This results demonstrate that the hybrid modelization for thin-walled stiffened structures can be beneficial for the shape sensing with the iFEM. In fact, this formulation allows to reach a significant accuracy with a more computationally efficient model and a slightly reduced number of strain sensors.

The use of hybrid shell-beam iFEM models should be further investigated in future works. In particular, the effect of different strain sensors' configurations and the possibility to further decrease the number of required sensors should be explored.

REFERENCES

[1] M. Gherlone, P. Cerracchio, and M. Mattone. Shape sensing methods: Review and experimental comparison on a wing-shaped plate. *Progress in Aerospace Sciences*, 99:14 – 26, 2018. doi:10.1016/j.paerosci.2018.04.001.

[2] T. Nakamura, H. Igawa, and A. Kanda. Inverse identification of continuously distributed loads using strain data. *Aerospace Science and Technology*, 23(1):75 – 84, 2012. doi:10.1016/j.ast.2011.06.012.

[3] R. Roy, M. Gherlone, C. Surace, and A. Tessler. Full-field strain reconstruction using uniaxial strain measurements: application to damage detection. *Applied Sciences*, 11(4), 2021. doi:10.3390/app11041681.

[4] L. Colombo, D. Oboe, C. Sbarufatti, F. Cadini, S. Russo, and M. Giglio. Shape sensing and damage identification with ifem on a composite structure subjected to impact damage and non-trivial boundary conditions. *Mechanical Systems and Signal Processing*, 148:107163, 2021. doi:10.1016/j.ymssp.2020.107163.

[5] M. Esposito and M. Gherlone. Material and strain sensing uncertainties quantification for the shape sensing of a composite wing box. *Mechanical Systems and Signal Processing*, 160:107875, 2021. doi:10.1016/j.ymssp.2021.107875.

[6] A. Tessler and J. L. Spangler. A variational principle for reconstruction of elastic deformations in shear deformable plates and shells. Report NASA/TM-2003-212445, NASA Langley Research Center, Hampton, VA, United States, 2003.

[7] M. Gherlone, P. Cerracchio, M. Mattone, M. Di Sciuva, and A. Tessler. Shape sensing of 3d frame structures using an inverse finite element method. *International Journal of Solids and Structures*, 49(22):3100–3112, 2012. doi:https://doi.org/10.1016/j.ijsolstr.2012.06.009.

[8] A. Tessler and J. L. Spangler. Inverse fem for full-field reconstruction of elastic deformations in shear deformable plates and shells. In *Proceedings of the 2nd European Workshop on Structural Health Monitoring*. Munich, 2004.

[9] H. Zhu, Z. Du, and Y. Tang. Numerical study on the displacement reconstruction of subsea pipelines using the improved inverse finite element method. *Ocean Engineering*, 248:110763, 2022. doi:10.1016/j.oceaneng.2022.110763.

[10] J. Wang, L. Ren, R. You, T. Jiang, Z. Jia, and G. xin Wang. Experimental study of pipeline deformation monitoring using the inverse finite element method based on the ibeam3 element. *Measurement*, 184:109881, 2021. doi:10.1016/j.measurement.2021.109881.

[11] R. Roy, M. Gherlone, and C. Surace. A shape sensing methodology for beams with generic cross-sections: Application to airfoil beams. *Aerospace Science and Technology*, 110:106484, 2021. doi:10.1016/j.ast.2020.106484.

[12] D. Oboe, L. Colombo, C. Sbarufatti, and M. Giglio. Shape sensing of a complex aeronautical structure with inverse finite element method. *Sensors*, 21(4), 2021. doi:10.3390/s21041388.

[13] A. Kefal, J. B. Mayang, E. Oterkus, and M. Yildiz. Three dimensional shape and stress monitoring of bulk carriers based on ifem methodology. *Ocean Engineering*, 147:256 – 267, 2018. doi:10.1016/j.oceaneng.2017.10.040.

[14] M. Esposito, M. Mattone, and M. Gherlone. Experimental shape sensing and load identification on a stiffened panel: A comparative study. *Sensors*, 22(3), 2022. doi:10.3390/s22031064.